AGU PUBLICATIONS

JGR

Journal of Geophysical Research: Earth Surface

RESEARCH ARTICLE
10.1002/2015JF003632

Root reinforcement of soils under compression

M. Schwarz[1,2], A. Rist[3], D. Cohen[4], F. Giadrossich[5], P. Egorov[3], D. Büttner[3], M. Stolz[3], and J.-J. Thormann[1]

[1]Department of Agronomy, Forestry, and Food Sciences, Bern University of Applied Sciences, Bern, Switzerland, [2]EcorisQ, Geneva, Switzerland, [3]Department of Architecture, Wood, and Civil Engineering, Bern University of Applied Sciences, Bern, Switzerland, [4]Department of Geological and Atmospheric Sciences, Iowa State University, Ames, Iowa, USA, [5]Department of Agriculture, University of Sassari, Sassari, Italy

Key Points:
- Root reinforcement has a major influence on soil compression behaviors
- The CoRoS model describes the force-displacement behavior of compressed rooted soils
- The CoRoS model can be used in an upscaling framework for slope stability

Correspondence to:
M. Schwarz,
massimiliano.schwarz@bfh.ch

Citation:
Schwarz, M., A. Rist, D. Cohen, F. Giadrossich, P. Egorov, D. Büttner, M. Stolz, and J.-J. Thormann (2015), Root reinforcement of soils under compression, *J. Geophys. Res. Earth Surf.*, *120*, 2103–2120, doi:10.1002/2015JF003632.

Received 10 JUN 2015
Accepted 3 SEP 2015
Accepted article online 8 SEP 2015
Published online 15 OCT 2015

Abstract It is well recognized that roots reinforce soils and that the distribution of roots within vegetated hillslopes strongly influences the spatial distribution of soil strength. Previous studies have focussed on the contribution of root reinforcement under conditions of tension or shear. However, no systematic investigation into the contribution of root reinforcement to soils experiencing compression, such as the passive Earth forces at the toe of a landslide, is found in the literature. An empirical-analytical model (CoRoS) for the quantification of root reinforcement in soils under compression is presented and tested against experimental data. The CoRoS model describes the force-displacement behavior of compressed, rooted soils and can be used to provide a framework for improving slope stability calculations. Laboratory results showed that the presence of 10 roots with diameters ranging from 6 to 28 mm in a rectangular soil profile 0.72 m by 0.25 m increased the compressive strength of the soil by about 40% (2.5 kN) at a displacement of 0.05 m, while the apparent stiffness of the rooted soil was 38% higher than for root-free soil. The CoRoS model yields good agreement with experimentally determined values of maximum reinforcement force and compression force as a function of displacement. These results indicate that root reinforcement under compression has a major influence on the mechanical behavior of soil and that the force-displacement behavior of roots should be included in analysis of the compressive regimes that commonly are present in the toe of landslides.

1. Introduction

Root reinforcement is a key factor contributing to the stability of vegetated steep slopes and plays an important role in determining the management of protection forests and bioengineering measures [*Stokes et al.*, 2014]. Most studies quantify root reinforcement from the point of view of the shear resistance of a rooted soil often implemented within an infinite slope stability analysis [e.g., *Wu et al.*, 1979; *Waldron and Dakessian*, 1981; *Bathurst et al.*, 2010]. Root reinforcement is included in the Mohr-Coulomb failure criteria as an additional root cohesion term usually homogeneously distributed across a vegetated slope with few studies considering the heterogeneous distribution of root reinforcement at the stand scale [e.g., *Kuriakose et al.*, 2008; *Schwarz et al.*, 2012b; *Hwang et al.*, 2015]. Even less work has been devoted to the role of root reinforcement in soils that are in compression as occurs at the toe of a shallow landslide. A unique study on root compression [*Wu et al.*, 1988] showed that the bending force of some roots in compression can be of the same order (~100 N) as that of a root in tension. Yet this aspect is entirely neglected in slope stability analysis of shallow landslides.

Three-dimensional limit equilibrium analyses [*Schwarz et al.*, 2010a; *Milledge et al.*, 2015] make a fundamental assumption that the sliding mass behaves as a rigid block neglecting the effects of local failures and the nonuniform stress fields and boundary conditions near the scarp and in the toe prior to landsliding [e.g., *Urciuoli et al.*, 2007]. During landslide initiation, a soil element may be in different stress configurations depending on its location: shear, tension, or compression. Figure 1 illustrates schematically the loading conditions of four soil volume elements during the triggering of a shallow landslide. Usually, for rainfall-triggered landslides, the initiation is caused by a local loss of shear strength (Figure 1, case 1) due to the combined effect of increased soil bulk density and either an increase in pore water pressure or a decrease in soil suction along the potential failure plane (indicated by a red curve in Figure 1). Once local failure occurs, the first evident sign of movement is observed by the formation of a tension crack in the upper part of the landslide (Figure 1, case 2). Simultaneously, the destabilized soil mass causes an increase in the lateral compressive stress in the

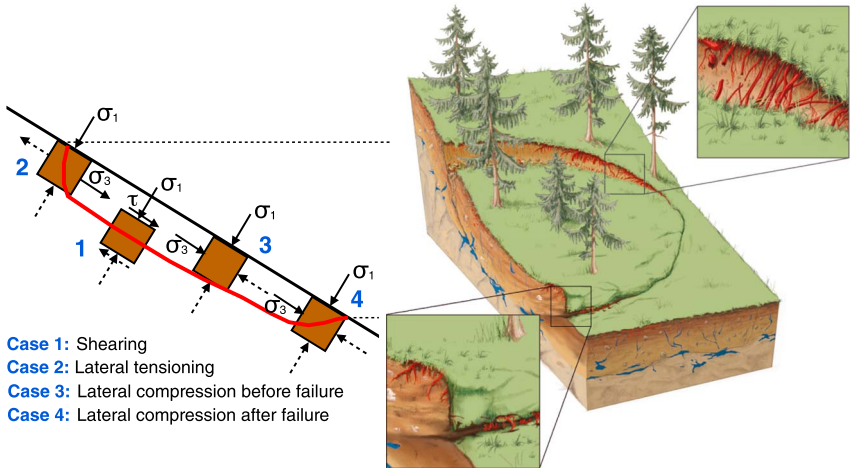

Figure 1. Activation of root reinforcement in tension crack (top inset) and in compression zone (bottom inset) during shallow landslide initiation. Left side image shows the representative soil volume elements under different stress configurations at different locations in the landslide.

downslope zone (Figure 1, case 3). Where the cumulative downslope lateral stress reaches a critical value the soil may fail, creating a failure surface (or band). Failing of the soil mass above the toe corresponds to compressive stress conditions as illustrated in Figure 1, case 4. The behavior of soils under these different stress conditions is usually tested in the laboratory with different stress tests.

The compressive stress condition illustrated in case 4, Figure 1, is similar to passive Earth pressure conditions discussed in geotechnical engineering in the context of the design of retaining walls. Passive Earth pressure state occurs if a wall moves downslope toward the adjacent backfill (Figure 2a), increasing pressure and inducing compressive lateral strains [*Kramer*, 1996]. If the wall moves sufficiently toward the backfill, the soil will fail in shear along the failure plane, a wedge will slide up that plane, and maximum passive pressure then acts on the wall. The pressure in the soil above the moving wall (Figure 2a) is called the active Earth pressure. Figure 2b shows the analogy between the retention wall and the toe of a failing slope. In the failing slope, the soil mass above the toe represents the wall that moves downslope creating passive Earth pressure condition and the failing wedge.

The first study that included compression within a three-dimensional limit equilibrium approach for the analysis of shallow landslides was that of *Terwilliger and Waldron* [1991]. They considered the lateral effects of active and passive Earth pressures on the top and the toe of a sliding block. Later on, *Puzrin and Schmid* [2007] implemented this concept in a numerical analysis for shallow and creeping landslides. Recently, *Milledge et al.* [2015] developed a multidimensional stability model for shallow landslide building up on the concepts proposed by *Terwilliger and Waldron* [1991] and applying the calculation of passive/active Earth pressures to include the effects of the upslope and the downslope soil block boundaries in the force balance calculations. Yet a systematic quantification and discussion of the passive Earth pressure on the triggering of shallow landslides is still missing.

Numerous approaches for estimating the value of the passive Earth pressure can be found in the literature going back to the eighteenth century. The most commonly used limit equilibrium approaches are those of Rankine [1857] and Coulomb [1776] (see *Bowles* [1996]). These approaches, however, overestimate the passive Earth pressure for wall frictions greater than zero [*Bowles*, 1996]. For this reason, *Caquot and Kerisel* [1948] produced tables of Earth pressure coefficient based on experiments with nonplanar failure surfaces. Later, *Janbu* [1957] and then *Shields and Tolunay* [1973] proposed an approach to the Earth pressure problem similar to the method of slices used in slope stability analysis. Recently, finite element methods were applied to test the validity of such approaches for different initial and boundary conditions [e.g., *Benmeddour et al.*, 2012]. All these new methods yield values for the passive Earth pressure coefficient smaller than that of Rankine or Coulomb. All methods mentioned above estimate a passive Earth pressure coefficient corresponding to the maximum possible mobilized force. The effect of displacement on passive Earth pressure was introduced more recently using empirical hyperbolic models calibrated with experimental data [*Duncan and*

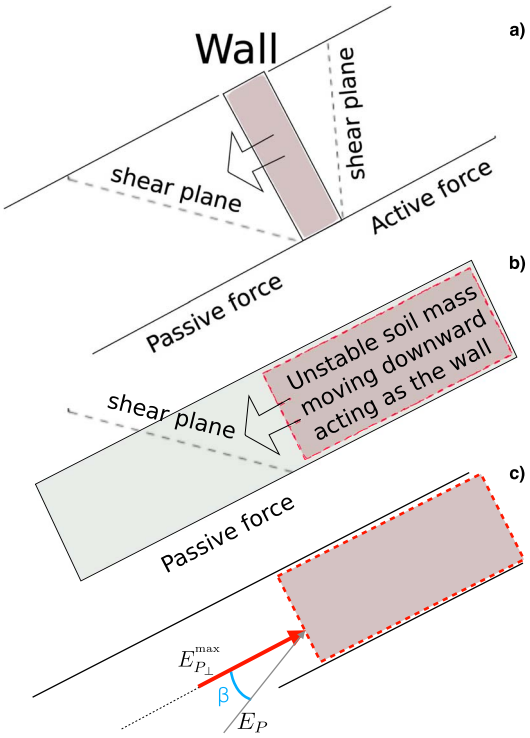

Figure 2. (a) Retention wall moving downslope creating passive Earth pressure condition in the downslope wedge and active pressure conditions upslope. (b) Analogy between the retention wall in Figure 2a and the unstable soil mass that moves downslope toward the toe (wedge). (c) Orientation of the E_P force vector and its inclination β relative to the analog wall activating the passive Earth pressure force.

Mokwa, 2001; *Shamsabadi et al.*, 2007]. These models, however, are not well suited for precompressed soils and cyclic stress conditions [*Cole and Rollins*, 2006] because in these situations, the passive Earth pressure curve has an inflection point that cannot be represented with hyperbolic models.

The effect of roots on the passive Earth pressure has always been neglected based on the assumption that the compressive strength of roots is low in comparison to that of soil [*Gray and Sotir*, 1996]. The first compression test of roots in the field was performed by *Wu et al.* [1988] who used a steel sleeve applied at the end of an exposed root on a soil profile to measure the compressive force in the direction perpendicular to the soil profile. In *Wu et al.* [1988]'s experiments, all roots failed by buckling. This pioneering work gave the first quantitative mechanical contribution of roots under compression: for root diameter of hemlock trees (*Tsuga sp.*) ranging between 2 and 9 mm, the maximum compression load reached values between 10 and 180 N. Roots crossing a shear plane induced by passive Earth pressure may behave differently than a single root pushed into the soil owing to different boundary conditions (the soil mass is also under compression and shearing). Furthermore, *Wu et al.*'s [1988] study made no link of this root reinforcement mechanism to slope stability.

To date, root reinforcement of soil is calculated for roots subjected to tension or pull out at the scarp or head of a slide, or in shear along a slide's basal failure surface. The most advanced models for estimating this root reinforcement use fiber bundle models [*Pollen and Simon*, 2005; *Schwarz et al.*, 2010b; *Cohen et al.*, 2011]. These models have shown that reinforcement may be quantified in terms of a maximum tensile force and a root bundle stiffness (the amount of root reinforcement mobilized per unit displacement) [*Schwarz et al.*, 2013a]. Furthermore, strain-controlled fiber bundle models [*Schwarz et al.*, 2013a] made clear that the so-called root apparent cohesion added to the soil cohesion in the Mohr-Coulomb formulation for soil strength is incorrect because root reinforcement depends on displacement and peak root reinforcement does not generally occur at the same displacement as the soil peak strength. These models supported the experimental results of early studies [*Pollen et al.*, 2004; *Docker and Hubble*, 2008; *Fan and Su*, 2008]. Fiber bundle models, however, have neither been adapted nor applied to roots in compression at the toe of a failing landslide.

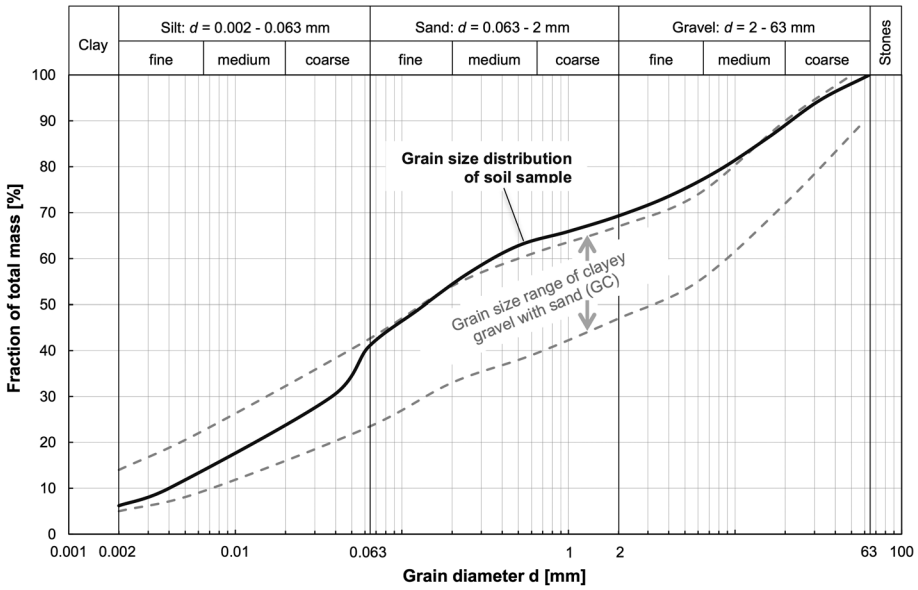

Figure 3. Grain size distribution of soil sample (solid black line) and typical grain size range of clayey gravels with sand (GC; gray dashed lines) according to USCS (SN 670004-2b).

The objective of this work is to measure, using laboratory experiments, the contribution of roots to the maximum passive Earth force and its evolution with displacement. Another objective is to formulate an empirical-analytical model for quantifying root reinforcement in soils under compression for conditions similar to those found at the bottom passive wedge at the toe of a shallow landslide. Sensitivity analyses of the model are also performed using field-measured root distributions in order to discuss the results in the context of slope stability assessment and protection forest management. The present work represents an important link, complementary to the formulation of root reinforcement in tension and shear [*Schwarz et al.*, 2013a], in the upscaling of root reinforcement from a root bundle to the hillslope scale [*Schwarz et al.*, 2010b] and the quantification of its effect on hillslope stability [*Schwarz et al.*, 2012a].

2. Laboratory Experiments

2.1. Materials and Sampling Site

Soil and root samples used in the experiments were excavated on a steep, 30°, north-facing slope on the Honegg ridge in the Emmental, Swiss Prealps. The site (UTM coordinates 629,370/185,050 zone 32; latitude 46.8160°N, longitude 7.8235°E) is located at an altitude of about 1000 m above sea level (asl). The climate is maritime, typical of central alpine north-facing slopes. Annual precipitation is about 1600 mm, and the mean annual air temperature is about 6 to 7°C (Metro Swiss, 2012, http://www.meteoschweiz.admin.ch/home/klima/vergangenheit/klimanormwerte/normwert-karten.html). The site is located in the Plateau Molasse at its southernmost limit to the folded-inclined Subalpine Molasse (clastic sedimentary rocks). The site is composed of Pleistocene moraine material originating from the last glacial maximum Emme glacier, now covered by Holocene weathered hillside regolith (geological map of Switzerland 1:25'000, Federal Office of Topography swisstopo, 2012). The soil layer is thus rich in rock fragments and only 30 to 50 cm deep. The low hydraulic conductivity of the moraine material favors wet conditions resulting in a slope gleysol and in local slope failures and scarps visible during the field campaign.

The site belongs to the montane altitudinal belt sustaining a conifer forest dominated by European spruce (botanical *Picea abies*). The phytosociological classification is a *Festuco-Abieti-Fagetum* mixed with *Aceri-Fraxinetum* and *Carici remotae-Fraxinetum*. The actual forest cover is composed of 70% European spruce and 30% silver fir (*Abies alba*). Forest canopy cover is about 80% and nearly homogeneous, interrupted only by small gaps (maximum 5 m in diameter). The mean tree height is about 25 m. Tree regeneration is dominated by silver fir (*Abies alba*) and sycamore maple (*Acer pseudoplatanus*) seedlings whose coverage ranges between 20 and 60%. The forest at the site is managed as a protection forest for slope stabilization and for soil protection from erosion in accord with the Swiss national directives [*Frehner et al.*, 2005].

Table 1. Mechanical Properties of the Soil Used for the Compression Experiments[a]

U.S. Geological Survey Soil Classification		GC
c_c	6.2	(% by mass)
c_M	34.6	(% by mass)
c_S	28.6	(% by mass)
c_G	30.7	(% by mass)
d_{60}	0.384	(mm)
d_{50}	0.143	(mm)
d_{30}	0.038	(mm)
d_{10}	0.004	(mm)
C_{Ud}	87.3	(–)
C_{Cd}	0.9	(–)
W_L	33.2	(% by mass)
W_P	22.5	(% by mass)
I_P	10.7	(% by mass)
W_{Pr}	15.3	(% by mass)
ρ_{Pr}	1.81	(g/cm^3)
D_{Pr}	86.7	(%)

[a]USCS = Unified Soil Classification System; GC = clayey gravel; c = content, indices *C*, *M*, *S*, and *G* mean clay, silt, sand, and gravel, respectively; *d* = grain diameter at the indexed fraction of total mass shown in the grain size distribution diagram; C_{Ud} = coefficient of uniformity; C_{Cd} = coefficient of curvature; *W* = water content; indices L, P, and Pr mean at the liquid limit, at the plastic limit, and at ρ_{Pr}; I_P = plasticity index; $D_{Pr} = (\rho_B/\rho_{Pr})$ 100 = degree of compression. The parameters W_{Pr} , ρ_{Pr}, and D_{Pr} are derived from a Proctor test according to SN 670330-2 on the material's fraction with $d < 4.0$ mm; W_L, W_P, and I_P are derived from testing the material fraction < 0.5 mm according to SN 670345-b. All other parameters are derived from testing the fraction < 0.5 mm according to SN 670004-2b.

2.2. Soil

One cubic meter of soil was excavated from the field site for analyses and experiments. The material was excavated from the A horizon within the top 0.4 m. The sampling site was representative of a landslide prone area. Soil samples were stored in a closed box during transport to the laboratory and remained sealed until analyses and experiments were performed. Grain size distribution, Atterberg's consistency limits, and Proctor compaction test to determine density and water content of soil subsamples were determined in the laboratory. In addition, shear parameters, i.e., the angle of internal friction and the cohesion, were measured as a function of water content by means of direct shear tests. The grain size analysis was performed according to the Swiss Norm SN 670004-2b and the determination of the consistency limits according to SN 670345-b, both of which are based on the Unified Soil Classification System (USCS). The soil was classified as a clayey gravel (GC) with sand. Grain size distribution is shown in Figure 3 and various parameter values are given in Table 1. Figure 3 shows that the grain size distribution slightly exceeds the upper limit of the typical GC band in the range between medium sand and medium gravel. Thus, naming convention adds the label "with sand" following the main soil group of clayey gravel. The derived parameter C_{Ud} (coefficient of uniformity) in Table 1 indicates that the soil is well graded and thus compressible. The low value of the plasticity index (IP, Table 1) reveals that the soil's consistency is sensitive to changes in water content. The Proctor test was performed according to SN 670330-2. The grain size fraction >4.0 mm was removed from the original material prior to the test in order to perform standardized analysis. That fraction was 25% of the material's total mass. The optimum water content, W_{Pr}, at the material's maximum density, ρ_{Pr}, proved to be 7% by mass lower than the plastic limit, W_P. The material's degree of compression, D_{Pr}, used for the lateral compression experiments with and without roots, is relatively low compared to materials used in geotechnical applications. However, this value is representative of a near-surface forest soil with small bulk density which is the focus of this paper.

Table 2. Soil Shear Parameters of the Fraction < 0.5 mm for Three Samples With Different Water Contents[a]

Sample	v (mm/s)	ρ_B (g/cm^3)	n (% by volume)	θ_g (% by mass)	θ_v (% by volume)	S_R (% by volume)	ϕ' (deg)	c' (kN/m^2)
1	0.04	1.57	41.96	19.43	30.45	72.52	23.7	21.6
2	0.04	1.56	42.07	22.84	35.72	84.9	24.1	18.1
3	0.04	1.56	42.41	27.22	42.33	99.81	27.1	13.5

[a] v is shearing rate; ρ_B is bulk density measured prior to the experiment when the soil was formed in the device; n is porosity; θ is water content with indices g and v indicating gravimetric and volumetric values, respectively; S_R is degree of saturation; ϕ' is effective angle of internal friction; c' is effective cohesion. The direct shear tests were performed in accordance with the standard DIN 18137.

The shear parameters were determined according to the standard DIN 18137 by means of the grain size fraction < 0.5 mm using a box shear apparatus (Wille Geotechnik, model SP 10) (see Table 2). After consolidating each sample for a minimum of 150 min, normal stresses σ' of 10, 20, 40, and 80 kPa were incrementally applied to obtain the shear strength, the effective angle of internal friction ϕ', and the effective cohesion c'. Low values of normal stress used in these tests are typical of low superimposed loads at small depth where shallow slope failures occur at this site. The maximum shearing rate to maintain drained conditions ($v = 0.04$ mm s^{-1}) was determined using the plasticity index (IP, Table 1) according to DIN 18137. Tests were performed at three water contents (Table 2): (1) the liquid limit W_L, (2) the plastic limit W_P, and (3) the mean field water content, $W_F = 19.2\%$ by mass, measured during sampling and experiments between June and August 2012.

2.3. Roots

Roots of European spruce (botanical *Picea Abies*) were cut from a depth between 0.1 and 0.4 m below the ground surface. Root diameters ranged between 1 mm and 30 mm, and root length was 1 m. Roots were wrapped in plastic foils in order to prevent them from drying during transport. In the laboratory, roots were stored in water at about 20°C and tested within a few weeks.

2.4. Experimental Setup and Procedures

The compression experiments using rooted and nonrooted soil samples were performed using an experimental setup specifically developed for this study (Figure 4). The device consists of two units: (1) a steel frame with a stiff plate 2 cm thick, 72 cm wide, and 38 cm high connected to in-feed slide to provide the compressive load; (2) a wooden frame containing the soil and roots to be compressed. Both units were held together by longitudinal tensioning thread bars during the compression experiments. The feed of the slide was controlled by four electrical jacks, two in series each on the left and right sides of the steel frame. Each jack can sustain a load of 2000 kg. One side wall of the frame is made of acrylic glass to allow direct observations of processes in the soil under compression. This wall and the one opposite were held together during the experiments by means of transverse tensioning bars (Figure 4).

In its initial state prior to an experiment, the compression plate was positioned at a distance of 100 cm from the rear wall on the opposite side. The soil was formed and compacted in three layers of about the same thickness up to a total height of 25 cm above the lower edge of the compression plate. The compaction was performed by a 10 kg, 24 cm long square plate placed horizontally on the soil surface and guided vertically by a cylindrical ram (dropped from a height of 0.4 m) to induce controlled energy impacts. For all experiments, the same soil material with the same dry weight but with varying water content was used. For each experiment, the soil was compacted to the same initial height on the same initial horizontal area, 72 cm wide and 100 cm long, and thus to the same total initial volume of 0.18 m^3 resulting in a constant dry bulk density ρ_B of 1.57 g/cm^3. To calculate ρ_B, the wet soil mass was weighed bucket by bucket when incorporated in the compression box prior to each experiment.

Rooted soil was simulated by incorporating roots between the first and second, and second and third soil layers, i.e., at about 8 cm and 16 cm above the lower edge of the compression plate. Table 3 shows the diameters of the five 1 m long roots used at each layer. Finding roots with similar diameters and lengths for both interfaces and for all experiments turned out to be not feasible. The total root mass of each layer varied with a relative standard deviation of about 11% within a single experiments (difference between upper and lower root layer), but less than 3% between the total root mass of the root bundles in the three experiments.

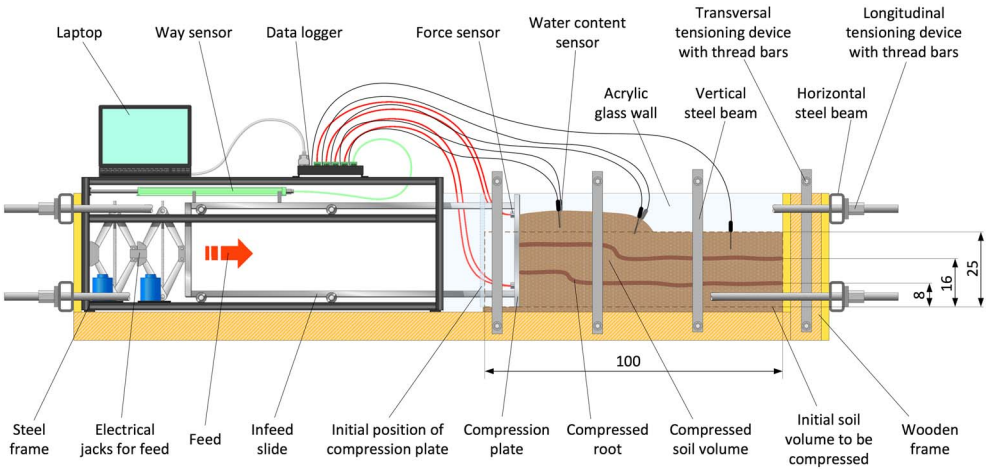

Figure 4. Side view of the experimental setup to compress rooted and nonrooted soils. Dimensions in centimeters. In the experiments, roots are not touching both sides of the wood box.

A displacement sensor (Burster GmbH, potentiometric displacement sensor model 8719, accuracy ±0.05%, Figure 4) was used to measure the relative horizontal displacement (Δx) of the compression plate. The sensor was calibrated prior to the experiments using five fixed points. The time dependent passive Earth pressure P_p was obtained by measuring the forces $F1$, $F2$, $F3$, and $F4$ on the four edges of the compression plate (Figure 5) using four load cells (Burster GmbH, miniature ring load cell model 8438, 50 kN, accuracy <1%). Each load cell was calibrated using known loads. Forces and displacements were recorded at time intervals of 1 s using a data logger (Campbell Scientific CR1000). The volumetric water content was monitored before and during compression at 1 min intervals at five positions near the soil surface (0–0.1 m) using Decagon 10HS soil moisture sensors (±3% accuracy by volume) (see Figures 4 and 5). Volumetric water content data were recorded using a Decagon Em50 data logger.

After forming the rooted (or nonrooted) soil in the box and placing the water content sensors in the soil, the compression experiment was started by activating the electrical jacks moving the compression plate toward the soil (mean velocities of 1.75 mm s^{-1}, within a range going from 1 to 3 mm s^{-1}). The total compression displacement achieved was at least 25 cm for each experiment. At displacements of 8 cm and 16 cm, experiments were paused to analyze both the dynamic and quasi-static forces. Motion was restarted after a minimum 1 min pause.

The measured forces were used to calculate the passive Earth pressure as a normal force per unit area. As all parameters were recorded as a function of time, the compression rate or velocity and acceleration could be derived as well as forces and stresses as a function of these variables.

To directly derive the roots's effect on the passive Earth pressure, experiments were executed pairwise, with and without roots incorporated in the soil, while the water content remained approximately constant for each pair: six experiments (LV3, LV4, LV5, LV6, LV7, and LV8) were performed at a mean initial volumetric water content representing typical field conditions ($\sim \theta_v = 0.29$).

Table 3. Root Diameters Used in the Soil Compression Experiments

Experiment	Layer Height (m)	Root Diameters (mm)
*LV*4	0.08	21, 18, 12, 10, 6
	0.16	23, 16, 12, 10, 6
*LV*6	0.08	28, 13, 13, 8, 5
	0.16	25, 15, 12, 10, 5
*LV*8	0.08	21, 15, 12, 10, 9
	0.16	21, 16, 12, 10, 8

3. Compressed Rooted Soil Model (CoRoS)

To quantify the force-displacement behavior of a rooted soil under compression, we developed an analytical model that considers root mechanical properties, root-size distribution, and soil mechanical properties and conditions. The contribution of roots to the total compressive force is considered additive to the compression force of the root-free soil.

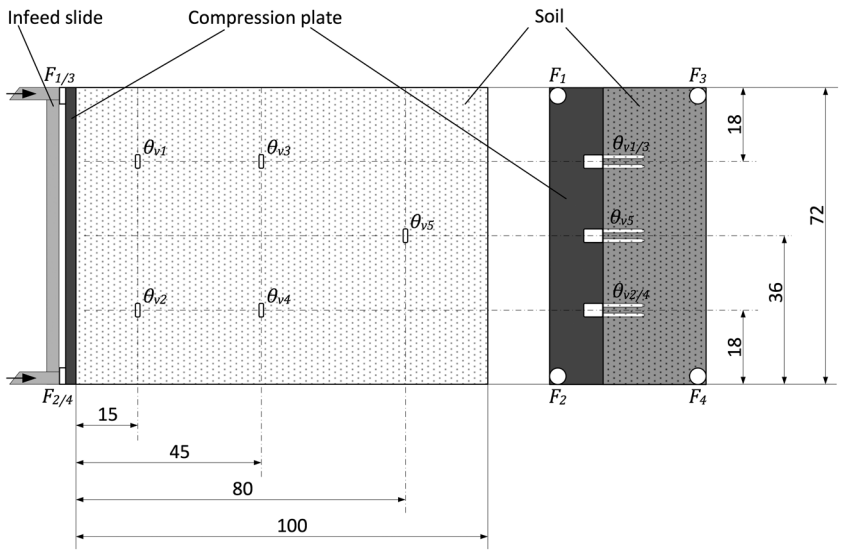

Figure 5. Positions of the four forces (F_i) and the water content ($\theta_v i$) sensors on the (left) base and (right) front of the device in its initial state prior to horizontal compression. Dimensions in centimeters.

3.1. Soil Compression

We estimated the maximum compressive resistance of the root-free soil from the maximum passive Earth pressure force. This force per unit length in the direction perpendicular to the wall (see Figure 2), $E_{P_\perp}^{\max}$, is given by [*Lang et al.*, 2003]

$$E_{P_\perp}^{\max} = \left(\frac{1}{2}\gamma H^2 K_P + 2c' H\sqrt{K_P}\right)\cos\beta, \tag{1}$$

where H is the soil depth perpendicular to soil surface, γ is the soil specific weight, c' is the effective soil cohesion, K_P is the passive Earth pressure coefficient, and β is the inclination of the passive Earth pressure force with respect to the surface perpendicular to the failure direction.

In the literature, β is assumed to have values between 0.7 and 0.9 of the value of the effective friction angle, ϕ' [*Lang et al.*, 2003]. The coefficient K_P, the ratio of horizontal to vertical effective stress, can be calculated following standard approaches for sloping walls and backfills [*Bowles*, 1996] or back calculated from field and laboratory experiments, as shown later in this work. For laboratory conditions, values of K_p can be estimated from the tables of *Caquot and Kerisel* [1948] or from the Coulomb approximation.

Classical geotechnical approaches usually assume quasi-static conditions when estimating the passive Earth pressure. During the triggering of a shallow landslide, the characterization of the passive Earth pressure mobilized may require the consideration of the rheological properties of the soil due to the acceleration of the soil mass. A rheological analysis of rooted soil goes beyond the aim of this paper, but we assume that the model presented here applies to different values of the passive Earth pressure force (E_P) whether under dynamical or quasi-static conditions. In what follows, we use the notation $E_{P_\perp}$ for the passive Earth pressure force perpendicular to the compression plate for both dynamic and quasi-static conditions.

As mentioned, empirically calibrated hyperbolic models have been used to characterize the behavior of the passive Earth pressure force with displacement [*Duncan and Mokwa*, 2001; *Shamsabadi et al.*, 2007]. Here we used the more flexible Weibull cumulative density function to characterize this behavior, i.e.,

$$E_{P_\perp}(\Delta x) = P_w(\Delta x)\, E_{P_\perp}^{\max}, \tag{2}$$

where Δx is the displacement and $P_w(\Delta x)$ is the Weibull cumulative density function given by

$$P_w(\Delta x) = 1 - e^{-(\Delta x/\mu)^\kappa}, \tag{3}$$

with κ being a constant exponent (the shape factor) and μ a scaling factor.

3.2. Root Reinforcement in Compression

We assumed that root reinforcement in a soil under compression is mobilized across the shear plane that develops during compression and leads to a complex bending-buckling-tensioning of the roots. The maximum compressive force of a buried root was obtained at the critical buckling condition. Assuming a beam-mode buckling, this condition could be derived from the theory of elastic stability [*Timoshenko and Gere*, 1961]. *Mitsuya et al.* [2013] used the formulation of *Timoshenko and Gere* [1961] for the computation of the critical axial load for buried pipelines. Here we applied it to a root of diameter Φ:

$$F_{cr}(\Phi) = \frac{\pi^2 EI}{l^2}\left(m^2 + \frac{b\,l^4}{m^2\pi^4 EI}\right), \tag{4}$$

where F_{cr} denotes the critical axial load, I is the second moment of area ($\pi\,\Phi^4/64$ for a circular root), E is the Young's modulus of the root [see *Schwarz et al.*, 2013a], l is the length of the root, m is the number of half-waves of buckling, and b is the soil elastic spring constant ($b = k_{soil}\,\Phi$, where k_{soil} is the unit spring constant of the soil in the lateral direction divided by the projected area of the root). The first term on the right-hand side of equation (4) can be interpreted as the buckling force due only to roots, whereas the second term represents the part of buckling force due to the radial soil constraint expressed by the spring constant k_{soil}. Setting k_{soil} to 0 implies that only root buckling contribute to reinforcement.

This equation is difficult to use for roots owing to its high number of unknowns (note that both E and I depend on root diameter usually through two-parameter power law functions) [e.g., *Schwarz et al.*, 2010a] and also because estimating the value of m requires iterating over the root diameter. To reduce the number of parameters for model calibration we assumed, like for the maximum force for roots in tension, that the maximum root-buckling force can be estimated as a function of root diameter using a two-parameter power law function

$$F_{max}(\Phi) = F_0\,\Phi^{\xi}, \tag{5}$$

where F_{max} is the maximum buckling-tensile force, ξ is an empirical exponent, and F_0 is a constant. We show later, in section 5.2, that this model gives good agreement with estimates using equation (4).

Root reinforcement in the compressed soil as a function of displacement can then be estimated using the fiber bundle model approach of *Schwarz et al.* [2013a] originally used for roots in tension but here adapted to roots in compression. The model, called RBMw (for Root Bundle Model Weibull), considers root diameter distribution and cumulative Weibull probability distribution of root strength within a single root diameter class. The total force (root reinforcement, F_{root}) of a bundle of roots is obtained by summing the force contributions of each root diameter class i ($F(\Phi_i, \Delta x)$) times a survival function, S, i.e.,

$$F_{root}(\Delta x) = \sum_{i=1}^{n_c} N_i\,F(\Phi_i, \Delta x)\,S(\Delta x_i^{\star}), \tag{6}$$

where n_c is the number of root diameter classes, N_i is the number of root in class diameter i, Φ_i is the diameter of root class i, and the star indicates that the displacement is normalized with respect to the displacement reached when the compression force is a maximum. The survival function, S, describes the increased probability that roots break with increasing displacement and has a Weibull distribution

$$S(\Delta x_i^{\star}) = \exp\left[-\left(\frac{\Delta x_i^{\star}}{\lambda}\right)^{\omega}\right], \tag{7}$$

where λ and ω are the scale and shape parameters, respectively, and λ is set to 1 (see *Schwarz et al.* [2013a] for further details).

In the rooted soil, individual root force as a function of displacement in compression, ($F(\Phi, \Delta x)$), is estimated using Hooke's law for elasticity, relating force to displacement through a spring constant that encapsulates the mechanical properties of the root-soil system under specific conditions (root diameter, tree species, stand, soil type, soil confining pressure, soil density, and moisture conditions). As implemented in the RBMw of *Schwarz et al.* [2013a],

$$F(\Phi, \Delta x) = k(\phi)\,\Delta x, \quad F(\Phi, \Delta x) < F_{max}(\Phi), \tag{8}$$

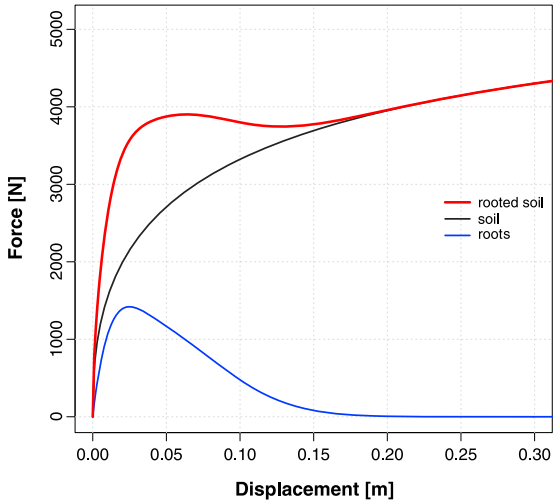

Figure 6. Modeled force-displacement curve for a rooted soil in compression (red curve) obtained by adding root-free soil compression model (black line) and the root reinforcement model (blue line). ($H = 0.25$ (m), $\phi' = 27$ (°), $c' = 13.5$ (kPa), $\rho = 1.5$ (t/m^3), $K_p = 12$ (–), $\mu = 0.12$ (m), $\kappa = 0.45$ (–), $F_o = 2.510^6$ (N), $\xi = 1.9$ (–), $k_i = 10^4$ (N m^{-1}), $k_p = 10^6$ (N m^{-2}), $\lambda = 1$ (–), $\omega = 1.8$ (–)).

where k is the spring constant. The relationship between spring constant and root diameter Φ is linear as shown from field pullout experiments [*Schwarz et al.*, 2011], i.e.,

$$k(\Phi) = k_i + k_p\,\Phi, \tag{9}$$

where k_i and k_p are the parameters of the linear regression. With this formulation,

$$\Delta x_i^{\star} = \frac{\Delta x_i\, k(\Phi)}{F_{\max}(\Phi)}. \tag{10}$$

The total compressive force for a rooted soil is then the sum of the soil and root compressive components. Combining equations (2) and (6), and considering a soil profile of width L onto which the passive Earth pressure is acting, yields

$$F_{\mathrm{CoRoS}}(\Delta x) = L\,P_w(\Delta x)E_{P_{\max}} + F_{\mathrm{root}}(\Delta x). \tag{11}$$

A sample calculation of the total compressive force is shown in Figure 6.

CoRoS model parameters were calibrated using the maximum-likelihood estimation method [*Beven*, 2009]. The parameters of the equation related to soil compression (K_p, μ, and κ) were calibrated based on the data from the laboratory experiments without roots (LV3, LV5, and LV7), whereas the parameters of the equation related to the root reinforcement (F_o, ξ, k_i, k_p, λ, and ω) were calibrated using the back-calculated root reinforcement obtained from the difference between the paired experiments with and without roots (LV4−LV3, LV6−LV5, and LV8−LV7). For the likelihood estimation method, we assumed a normal distribution of the residuals with a minimum of 10,000 combinations of parameter sets.

4. Results

4.1. Compression Experiments

Six-paired soil compression experiments (with and without roots) were performed. Root sizes used for the three-rooted soil experiments are shown in Table 3. The comparison between rooted and nonrooted conditions yields a quantitative characterization of the effects of root reinforcement under the specific combination of boundary and initial conditions. Figure 7 shows the force-displacement curves for all the experiments. In all experiments, the passive force increased nonlinearly with increasing displacement and tends to converge to a value ranging between 8 and 9 kN at a displacement of 0.15 m. The drop in the value of the lateral force

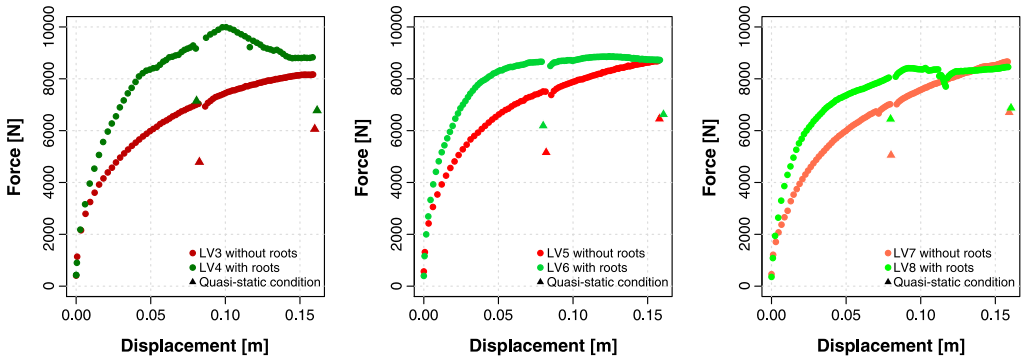

Figure 7. Force-displacement curves of all laboratory experiment pairs. Legend indicates test number (3 to 8) and type of test (with or without roots). The gap in the data at 0.08 m displacement is due to a pause during loading to obtain quasi-static conditions (triangles).

at regular displacement intervals corresponds to a 1 min pause in the load (zero strain rate). The triangles in Figure 7 indicate the values of the force measured at the end of the pause. The resulting quasi-static compression forces were about 20% lower than dynamic forces at 1.75 mm s^{-1} displacement rate, and the difference between quasi-static and dynamic forces was independent of the presence of roots.

Measurements of volumetric water content indicated that it increased during the compression experiments but no discernible difference was observed between the root-free and root-permeated soils.

4.2. CoRoS Model Calibration

Fitting of equations (1) and (3) for the root-free soil compression force yielded $K_p = 22.35$, $\mu = 0.07$ m, and $\kappa = 0.58$ with a standard deviation of 172 N. Figure 8 shows the data of the root-free soil compression for experiments LV3, LV5, and LV7 (gray dots) and the fitted model (solid red curve) with the corresponding 95% confidence interval (dashed red curves). The model yielded remarkable good agreement with the data. The narrow band of the confidence interval indicates that variability of the experimental results is low under similar conditions (initial compaction, displacement rate, and soil water content) and that replicated results are consistent.

Figure 9 shows the differences between paired root and root-free experiments. The results of the model fit are shown with solid curves and the 95% interval of confidence with dashed curves. The measured maximum

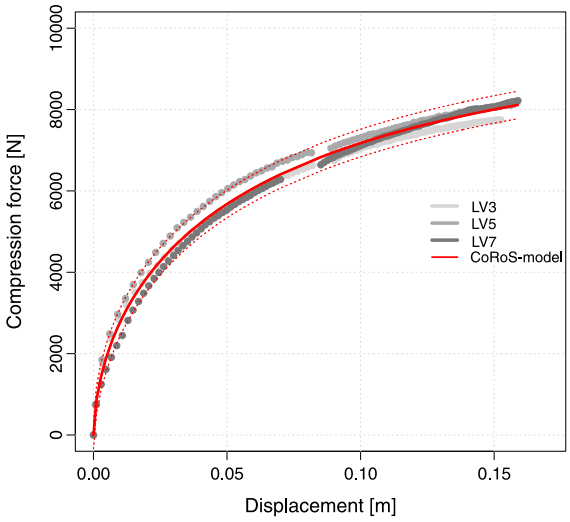

Figure 8. Comparison between force-displacement measured in the laboratory for root-free soil (LV3, LV5, and LV7, gray dots) and the fitted CoRoS model (red solid curve with confidence interval in red dotted curve).

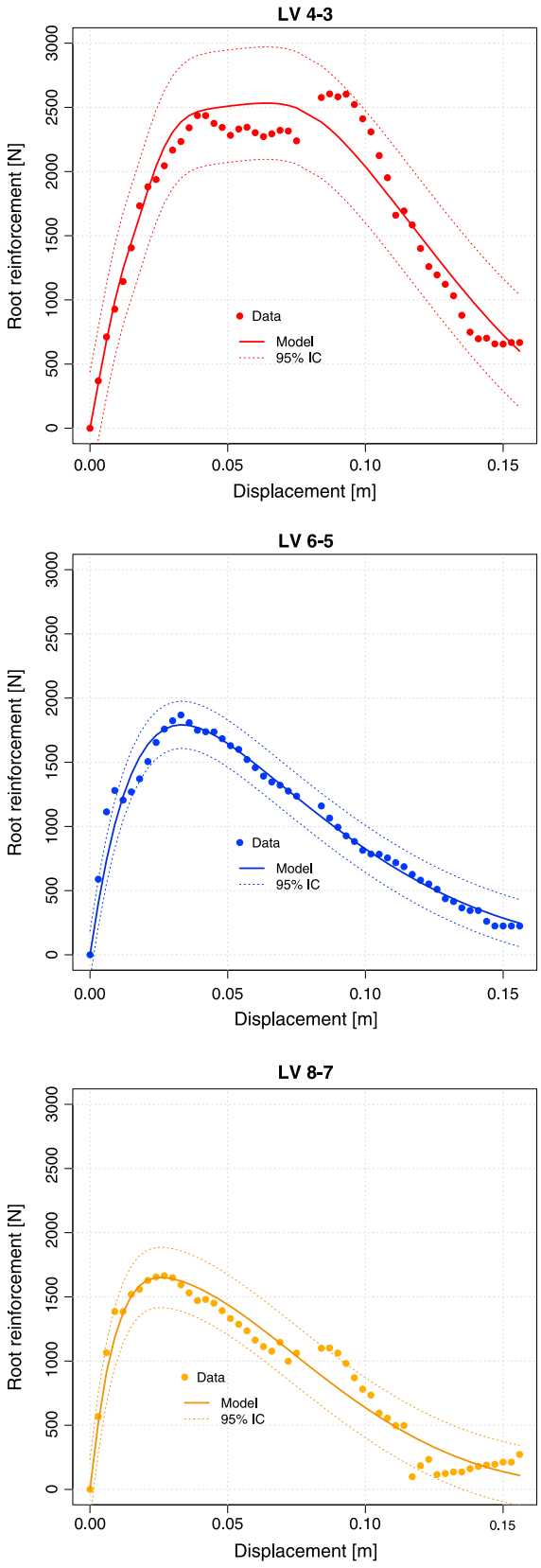

Figure 9. Force-displacement curves for root reinforcement obtained by subtracting rooted from nonrooted soil force compression between paired experiments (symbols) and comparison with CoRoS model (solid line) with 95% confidence interval (dotted lines).

Table 4. Parameters of the RBMw Model Calibrated Using Either Paired Laboratory Experiments or the Combination of All Experiments

Exp. Pair	F_0 (N)	ξ (–)	k_i (N m^{-1})	k_p (N m^{-2})	ω (–)	SD[a] (N)
LV4–LV3	26.5×10^5	1.94	9.6×10^3	1.4×10^5	3.3	223
LV6–LV5	17.3×10^5	1.92	2.6×10^3	8.7×10^5	1.4	85
LV8–LV7	24.5×10^5	1.98	15.9×10^3	5.7×10^2	1.8	125
Combined	6.5×10^5	1.67	4.8×10^2	10.2×10^5	1	470

[a]SD = standard deviation.

root reinforcement in all three experiments ranged between 1.7 and 2.6 kN and was mobilized at displacements between 0.03 and 0.05 m. Table 4 gives the fitted values of the parameters of the model (equations (6), (8), and (10)) for each paired experiment and for all experimental data combined together (one set of parameters fitted for all the experimental data sets). Figure 10 shows the results of equation (5) using the back-calculated values of the parameters from the experiments compared with the results of equation (4) assuming published values of E [*Schwarz et al.*, 2010b] and k_{soil} [*Mitsuya et al.*, 2013].

5. Discussion

5.1. Passive Forces

Our results show minimal differences in the values of the passive Earth pressure measured in the three compression experiments without roots indicating good reproducibility of the mechanical behavior of the soil despite small (less than 3%) variations in initial soil volumetric water content. For root-permeated soils, reproducibility is a greater challenge: obtaining roots of similar diameter from the same study area was a time consuming task necessitating numerous excavations. Even for roots of similar sizes (see Table 3), the variation of root strength found in field specimens yielded measurements of the passive Earth pressure force that have great variability (>50%, see Figure 9).

The shape of the passive Earth pressure curve measured in our experiments for root-free soil is comparable to that of loose soil described in the literature. For example, *Gutberlet et al.* [2013] presented results of lateral compression tests for homogeneous quartz sand and crushed gabbro showing different behaviors for loose (density of about 1.5 g cm^{-3}) and dense (density of about 1.7 g cm^{-3}) soils. The authors concluded that for loose sands no distinct peak in the mobilization curve occurs and critical state is approached asymptotically after a large displacement. For dense sands, *Gutberlet et al.* [2013] observed a peak in the compression force. Our results with loose soil show that, even for displacements larger than commonly found in the

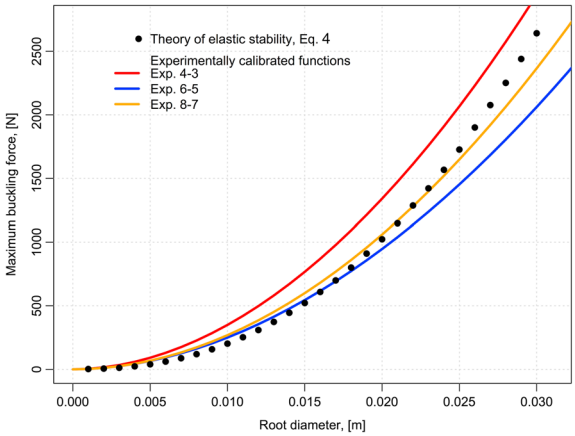

Figure 10. Maximum buckling force as a function of root diameter for theoretical calculated values (black dots, equation (4)) and the experimentally calibrated function (equation (5), red, blue, and orange curves). The Young's modulus, in Pa, was calculated as $E = 0.248 \times 10^8 \Phi^{-0.3}$, whereas k_{soil} was estimated using equation (13) in *Mitsuya et al.* [2013]: $k_{soil} = \frac{(0.36 \times 10^6)}{((0.17+0.83(0.02\Phi/0.1))0.1)}$, where k_{soil} and Φ have units of N m^{-3} and m, respectively.

literature (up to 0.15 m, compared with only a few millimeters in other studies), the passive Earth pressure force continued to increase (Figure 7). We attribute this behavior to the boundary conditions imposed by the test configuration: by constraining the motion of the compression plate in the horizontal direction, we observed (through the transparent side plate) the formation of new failure surfaces created sequentially with increasing displacement. With new failure surfaces, more soil was pushed by the plate and this caused an increase of the compression force due to the accumulation of soil in front of the plate.

The results of *Gutberlet et al.* [2013] and that of others [e.g., *Wilson and Elgamal*, 2010] indicate that the peak in the compression force occurs at a ratio of displacement to wall height of about 1 to 3%. The analysis of *Gutberlet et al.* [2013] showed that the formation of a distinct shear band is well defined at small displacements (22 mm corresponding to about 1% of the wall height). Assuming a value of 1% corresponds to a displacement of 0.025 m in our experiment which corresponds to the displacement at which maximum root reinforcement is activated (see Figure 9).

At the toe of a shallow landslide, the passive Earth pressure condition exerted by the wall represented by the soil above the failing wedge (see Figure 2) is not constrained in the vertical direction as it was in our experiments. To allow for the vertical displacement of the compression plate, *Wilson and Elgamal* [2010] fitted each jack with a Teflon pad acting on a greased smooth steel plate attached to the wall. The results of Wilson's tests on dense sand showed a peak of strength at about 3.5% of the normalized displacement (displacement over wall height) and a wall uplift of the order of 3–5 mm (for a wall height of 1.68 m). These results showed that the residual passive forces at larger displacements decrease slightly (data available only up to 0.2 m horizontal displacement). Thus, at the toe of a shallow landslide, we should expect failure to occur along a single shear band and the passive Earth pressure to decrease at large displacements even for loose soils.

The passive Earth pressure depends not only on soil type and soil density but also on soil moisture. Compression experiments by *Poterasu* [2013] showed that pore volume saturation ranging from 5% to 100% associated with varying fractions of Kaolin clay content (6 to 10%) had major effects on the passive force behavior of the soil. The author argued that collapsing mechanisms of the clay-water bridges between the grains of the granular material were responsible for a significant reduction in soil stiffness and strength. Results from our experiments show that during compression water content increased probably due to the reduction of pore volume (contraction). Observed contraction following dilation associated with aggregate crushing has been shown to cause excess pore pressure [*Iverson et al.*, 2010] and may be responsible for soil weakening and landslide acceleration [*Iverson et al.*, 2000]. *Iverson et al.* [2000] field-scale landslide experiments demonstrated the sensitivity of landslide rates and styles to initial soil porosity and pore volume dilation/contraction. Roots may also affect soil contraction. By analogy with the effect of aggregates on soil water pressure and porosity, we hypothesize that the presence of roots in the soil influences postdilative contraction, soil hydraulic diffusivity, and also shear zone thickness. Thus, roots can affect the contraction rate and soil strength during the initial phases of shallow landslide triggering.

Our results also indicate that for displacement rates of 1 to 2 mm s^{-1}, the dynamic forces were about 30% higher than quasi-static ones, reached when pausing the strain loading for 1 min, and that the reinforcement due to roots was independent of the rate of displacement (see Figure 7). A comparison of these results with other literature studies is difficult because strain rate is usually not discussed in similar compression experiments [e.g., *Poterasu*, 2013; *Wilson and Elgamal*, 2010].

A comparison between our estimated value of the passive Earth pressure coefficient, K_P, and values obtained with other methods is difficult. In our experiments, we estimated K_P as an empirical parameter which contains the effects of plate movement (horizontal versus parallel to shear surface), displacement rate, and soil cohesion. Classical methods such as Rankine or Coulomb, however, assume only horizontal displacement, quasi-static conditions, no soil cohesion (implemented in the calculation of Earth pressure), and a constant residual value of passive Earth pressure that considers only the mobilization of shear forces along a single surface. Calculations of K_P using Rankine's and Coulomb's methods for the conditions of our compression tests lead to values of 2.7 and 3.9, respectively, and yield passive compression force values of 6.1 and 7.6 kN, respectively, when using equation (1). These values are similar to values measured for quasi-static conditions at 0.16 m displacement (see Figure 7). For cohesive materials, the passive Earth pressure estimated according to the model of *Mazindrani and Ganjali* [1997] yields $K_P = 121.4$ (with H=0.25 m, $\phi' = 27.1°$, and $c' = 13.5$ kPa) with an estimated force of 7.6 kN.

Our model fit of our data yields a standard deviation of about 2% of the maximum measured compression force (Figure 8). Fitting of the parameters tends to converge to a single solution (single maximum peak of the maximum-likelihood estimation model) indicating that the Weibull form of the model is well suited to reproduce the compression behavior of loose root-free soils. Analog three-parameter hyperbolic models such as the ones proposed by *Shamsabadi et al.* [2007] or *Duncan and Mokwa* [2001] could also have been used. However, the use of a Weibull cumulative density function in the CoRoS model adds more flexibility in the fitting of the model to the data.

5.2. Effects of Roots on Passive Earth Pressure

Results of paired experiments show, for the first time, how roots affect the strength of a rooted soil in compression. The most important effect is the increase of the passive Earth pressure force, up to displacements of 0.18 m (see Figure 7). The consequence of the addition of the buckling load of roots to the soil passive Earth pressure force is the increase of the apparent stiffness of the rooted soil.

The increase in the passive Earth pressure force could be due to several factors: bending during the initial development of the shear band, buckling under compression with increased shear displacement along the failure plane, and tension at even larger displacements. *Wu et al.* [1988] argued that, despite their high compressive strength, roots in soils in compression fail by buckling because of the low-confining pressure in the soil. Our measurements also support the assumption that buckling dominates over other mechanisms. Comparison of our empirical model for the maximum force held by roots in compression (equation (5)) with the theoretical buckling model of *Mitsuya et al.* [2013] (equation (4)) yields remarkably good agreement (Figure 10). This result upholds that buckling is the dominant root reinforcement in compression and validates our simple empirical two-parameter model as an alternative to the more complex theoretical buckling model.

Comparing the values of the fitted parameters in this study (parameters in equation (5)) with the values of previous studies [e.g., *Schwarz et al.*, 2013a] shows that the combined buckling-tension strength is 1 order of magnitude lower than the tension strength found for single roots. The back-calculated values of the Weibull exponent (that characterized the variability of root strength with lower values indicating more variability) range from 1.2 to 1.8, slightly less than the values found for tensile and pullout tests [*Schwarz et al.*, 2013a; *Vergani et al.*, 2014].

Root reinforcement in compression as a function of displacement shows a similar behavior to root reinforcement in tension and shearing, confirming our model assumption. This also applies to the progressive failure of roots with increasing displacement. Indeed, one can expect that for roots that grow in situ the amount of reinforcement they provide to the soil will be higher due to better anchoring of the roots in the soil. Moreover, root orientation in relation to the compression direction will also have an impact on the root reinforcement, but this effect is de facto included in our model that describes the maximum compressive root reinforcement as a function of root diameter (equation (5)).

The depth of roots in the soil profile will considerably influence the effects of root reinforcement on passive Earth pressure forces and the overall behavior of soils in compression. By analogy with the results of *Gutberlet et al.* [2013] that show how the global behavior of passive Earth pressure is dominated by the characteristics of the bottom layer of the soil (soil type, soil compaction, water content, root distribution), one should expect the contribution of root reinforcement to depend on how roots are distributed vertically along the soil profile. More studies are needed to test this hypothesis.

5.3. Sensitivity Analysis of Root Reinforcement Calculations

The RBMw gives an explicit formulation of the force-displacement behavior of a root bundle and considers the effect of root mechanical variability using a Weibull survival function. This Weibull formulation becomes increasingly realistic with a large number of roots. The maximum-likelihood approach for the estimation of the parameters yields a goodness of fit expressed as a standard deviation of the residuals of the model (see Table 4). Model calibration yielded a standard deviation of the order of 7 to 9% of the calculated maximum root reinforcement for all three data sets (see Figure 9).

Because root reinforcement strongly depends on root distribution, we assessed the sensitivity of the model using four different root distribution data sets obtained from 12 soil pits in the same study area (see *Schwarz et al.* [2012a, Figure 4] for details). We use the calibrated model parameters estimated from the combined laboratory experiments (combined data in Table 4). This calculation allows us to scale our laboratory measurements to the level of the root system of a single tree for root distributions measured at three

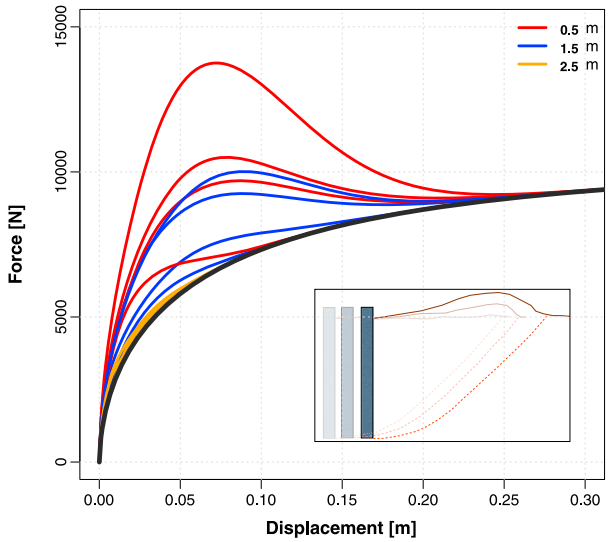

Figure 11. Force-displacement curves for rooted soil in compression for the type of failure that assume horizontal displacement of the compression plate. Curves are computed using model parameters calibrated for the combined laboratory data and field-measured root distributions for four different tree trunks at three distances: 0.5 m (red), 1.5 m (blue), and 2.5 m (orange). The black line shows the computed root-free soil force. A qualitative illustration of three arbitrary shapes of slip and top surfaces is shown in inset based on laboratory observations.

distances from the tree stem (0.5, 1.5, and 2.5 m). Figure 11 shows the results for boundary conditions identical to our laboratory experiments where the compression plate can only move horizontally (see inset of Figure 11). Under these conditions, once passive force is mobilized along the initial failure surface, the passive Earth pressure force continues to increase with displacement owing to the creation of additional failure surfaces and the accumulation of soil material in front of the moving plate.

For these simulated compression conditions, maximum root reinforcement varies between 0.5 and 7 kN at displacements ranging from 0.02 to 0.07 m. Root reinforcement increases with decreasing distance from the tree stem. The high variability of root reinforcement is due to the root distribution that differs for each tree. This variability exceeds 6 kN between the lowest and the highest values at 0.5 m distance from the tree stem (Figure 11, red curves) when root density is highest and decreases away from the tree stem when roots are fewer.

In our study we focused the analysis on a limited range of root diameters with a maximum diameter of 28 mm for the laboratory experiments. The largest root diameter considered for the sensitivity analysis shown in Figure 11 is 38 mm (measured at 1.5 m distance from a spruce stem with a diameter at breast height, DBH, of 0.2 m). At such short distances from the tree stem, these structural roots are supposed to, as primary function, stabilize the tree and have tended to be neglected in slope stability calculations as discussed in *Schwarz et al.* [2010b]. However, for certain tree species managed as coppice wood, the importance of such structural roots (sometimes larger than 50 mm) should be discussed in view of rooted soil stiffness and strength under compression. By analogy with the stabilization effects of slope grids [*Zeh*, 2007], a regular network composed of coppiced tree stumps has a major contribution on the stability of a slope due to the stiffness of the rooted soil material. It is also possible that these structural roots perform a function similar to soil nails as these central roots may penetrate to some depth and protrude beneath the base of the slip surface. More discussion on the role of structural roots on slope stability and additional research is needed to quantify their spatiotemporal effects.

5.4. From the Laboratory to a Rooted Slope: Upscaling Issues and Modeling Framework

The characterization of the triggering mechanisms of shallow landslides is found in a wide range of studies that goes from laboratory [*Iverson et al.*, 2010] and field experiments [*Askarinejad et al.*, 2012] to quantification methods such as limit equilibrium approaches and numerical analyses (finite elements and discrete element method). However, the coupled nature of the processes involved makes it difficult to fully describe this complexity, and simplifications are needed to make progress in the analysis. Some of the major issues related to this topic are the upscaling of spatiotemporal heterogeneities (e.g., root reinforcement, hydrological

processes, and soil evolution). While hydrogeological and other subsurface features are difficult to characterize for large areas, the analysis of vegetation cover, via light detection and ranging or stereo analysis, offers the possibility to infer the subsurface heterogeneity of related factors (i.e., root reinforcement). The present work is part of a multiscale framework to implement root reinforcement in slope stability calculations. The general structure of an upscaling framework was described by *Schwarz et al.* [2010b] and later extended with the use of the fiber bundle model for the quantification of root reinforcement under tension and shearing [*Schwarz et al.*, 2013a]. Field campaigns for the characterization of root distribution of different tree species in Alpine regions were carried out by *Schwarz et al.* [2012a, 2013b] and *Vergani et al.* [2014]. Finally, an implementation of root reinforcement in a discrete element model is expected to improve the quantification of the protective effect of vegetation against shallow landslide hazards. In particular, the consideration of displacement in the force balance calculation of slope stability analysis is expected to improve modeling results. Including displacement in calculations prevents making the common erroneous assumption that maximum active and passive Earth pressure forces take place at the same moment (and are then usually added). This assumption induces considerable error in the force balance, as shown experimentally by *Askarinejad et al.* [2012]. Results presented here contribute to quantify this error and introduce a realistic displacement-dependent model for forces (with or without roots) to use in numerical models. Further studies are needed to assess the variability of behaviors under real conditions and define the range of parameters values that may be applied.

6. Conclusions

The present study shows that root reinforcement for realistic root distributions has a major effect on the stiffness and strength of rooted soils under compression. The magnitude of root reinforcement strongly depends on root distribution and thus can have a high spatial variability at the hillslope scale. We presented a new empirical-analytical model (CoRoS) to quantify the force-displacement behavior of rooted soils under compression. The model can easily be included in an upscaling framework for slope stability calculations. Laboratory results show that adding 10 roots with diameters ranging from 6 to 28 mm in a rectangular soil profile 0.72 m by 0.25 m increased the compression resistance of the soil by 2.5 kN (40%) at a displacement of 0.05 m. Moreover, the apparent stiffness of the rooted soil was proved to be 38% higher than for the root-free soil (237 kN m^{-1} instead of 171 kN m^{-1}, respectively, for a soil 1 m in width). Calculated values of root reinforcement under compression using the CoRoS model calibrated with laboratory data and using field-measured root distribution indicate a maximum increase in the compression force of about 10 kN for a soil 1 m wide at a distance of 1.5 m from the trunk of spruce trees with a diameter at breast height of 0.2 and 0.4 m. The magnitude of root reinforcement decreases nonlinearly with increasing distance from the tree stem. At distances larger than 2.5 m (tree DBH: 0.2, 0.22, 0.37, and 0.37 m), no considerable root reinforcement under compression was observed. The quantitative analysis presented in the paper indicates that for realistic conditions, the magnitude of root reinforcement under compression has a major influence on the mechanical behavior of soils (up to 100%, see values shown in Figure 11). In view of these new results, we argue that the magnitude and spatial distribution of root reinforcement under compression has a major influence on the redistribution of forces in an unstable slope and thus should be considered in slope stability analyses. The results and modeling approach represent an important step toward a more realistic implementation of root reinforcement in slope stability calculations.

Acknowledgments
We thank Bruno Fritschi for his contribution to sensor installation, and Manfred Muhr and Fritz Muralt for the construction of the instrument compression frame. We thank the research fund of the Bern University of Applied Sciences for financing the "CoRoS" project. Laboratory data are freely available and may be obtained by contacting the first author. We thank anonymous reviewers and the Associated Editor for their constructive reviews and suggestions.

References

Askarinejad, A., F. Casini, P. Bischof, A. Beck, and S. M. Springman (2012), Rainfall induced instabilities: A field experiment on a silty sand slope in northern Switzerland, *Riv. Ital. Geotech.*, *3*, 50–71.

Bathurst, J. C., C. I. Bovoloa, and F. Cisneros (2010), Modelling the effect of forest cover on shallow landslides at the river basin scale, *Ecol. Eng.*, *36*, 317–327.

Benmeddour, D., M. Mellas, R. Frank, and A. Mabrouki (2012), Numerical study of passive and active Earth pressures of sands, *Comput. Geotech.*, *40*, 34–44.

Beven, K. (2009), *Environmental Modelling: An Uncertain Future?*, 310 pp., Routledge, London.

Bowles, J. E. (1996), *Foundation Analysis and Design*, McGraw-Hill, Singapore.

Caquot, A., and J. Kerisel (1948), *Tables for the Calculation of Passive Pressure, Active Pressure and Bearing Capacity of Foundations*, Gauthier-Villars, Paris.

Cohen, D., M. Schwarz, and D. Or (2011), An analytical fiber bundle model for pullout mechanics of root bundles, *J. Geophys. Res.*, *116*, F03010, doi:10.1029/2010JF001886.

Cole, R. T., and K. M. Rollins (2006), Passive Earth pressure mobilization during cyclic loading, *J. Geotech. Geoenviron. Eng. ASCE*, *132*, 1154–1164.

Docker, B. B., and T. C. T. Hubble (2008), Quantifying root reinforcement of river bank soils by four Australian tree species, *Geomorphology*, *100*, 401–418.

Duncan, J. M., and R. L. Mokwa (2001), Passive Earth pressures: Theories and tests, *J. Geotech. Geoenviron.*, *127*(3), 248–257.
Fan, C. C., and C. F. Su (2008), Role of roots in the shear strength of root-reinforced soils with high moisture content, *Ecol. Eng.*, *33*, 157–166.
Frehner, M., B. Wasser, and R. Schwitter (2005), Nachhaltigkeit und Erfolgskontrolle im Schutzwald [Sustainability and control method in protection forests]. Wegleitung fr Pflegemassnahmen in Wldern mit Schutzfunktion. Bundesamt fr Umwelt, Wald und Landschaft, Bern, Switzerland, 564 pp.
Gray, D. H., and R. B. Sotir (1996), *Biotechnical and Soil Bioengineering Slope Stabilization: A Practical Guide for Erosion Control*, Wiley-interscience, New York.
Gutberlet, C., R. Katzenbach, and K. Hutter (2013), Experimental investigation into the influence of stratification on the passive Earth pressure, *Acta Geotech.*, *8*, 497–507.
Hwang, T., L. E. Band, T. C. Hales, C. F. Miniat, J. M. Vose, P. V. Bolstad, B. Miles, and K. Price (2015), Simulating vegetation controls on hurricane-induced shallow landslides with a distributed ecohydrological model, *J. Geophys. Res. Biogeosci.*, *120*, 361–378, doi:10.1002/2014JG002824.
Iverson, R. M., M. E. Reid, N. R. Iverson, R. G. LaHusen, M. Logan, J. E. Mann, and D. L. Brien (2000), Acute sensitivity of landslide rates to initial soil porosity, *Science*, *290*, 513–516.
Iverson, N. R., J. E. Mann, and R. M. Iverson (2010), Effects of soil aggregates on debris-flow mobilization: Results from ring-shear experiments, *Eng. Geol.*, *114*, 84–92.
Janbu, N. (1957), Earth pressure and bearing capacity calculations by generalized procedure of slices, *Proceedings of the 4th International Conference on Soil Mechanics and Foundation Engineering, London*, vol. 2, pp. 207-12.
Kramer, S. L. (1996), *Geotechnical Earthquake Engineering*, 653 pp., Prentice-Hall, Upper Saddle River, N. J.
Kuriakose, S. L., V. G. Jetten, C. J. Van Westen, G. Sankar, and L. P. H. Van Beek (2008), Pore water pressure as a trigger of shallow landslides in the Western Ghats of Kerala, India: Some preliminary observations from an experimental catchment, *Phys. Geogr.*, *29*, 374–386.
Lang, H. J., J. Huder, and P. Aman (2003), *Bodenmechanik und Grundbau*, 320 pp., Springer, Berlin.
Mazindrani, Z. H., and M. H. Ganjali (1997), Lateral Earth pressure problem of cohesive backfill with inclined surface, *J. Geotech. Geoenviron.*, *123*, 110–112.
Milledge, D. G., D. Bellugi, J. McKean, A. L. Densmore, and W. J. Dietrich (2015), A multidimensional stability model for predicting shallow landslide size and shape across landscapes, *J. Geophys. Res. Earth Surf.*, *119*, 2481–2504, doi:10.1002/2014JF003135.
Mitsuya, M., T. Sakanoue, and H. Motohashi (2013), Beam-mode buckling of buried pipeline subjected to seismic ground motion, *J. Pressure Vessel Technol.*, *135*, 021801.
Pollen, N., A. Simon, and A. Collison (2004), Advances in assessing the mechanical and hydrologic effects of riparian vegetation on stream bank stability, in *Riparian Vegetation and Flivual Geomorphology*, vol. 8, edited by S. J. Bennett and A. Simon, pp. 125–139, Water Sci. Appl. Ser., AGU, Washington, D. C.
Pollen, N., and A. Simon (2005), Estimating the mechanical effects of riparian vegetation on stream bank stability using a fiber bundle model, *Water Resour. Res.*, *41*, 11–21, doi:10.1029/2004WR003801.
Poterasu, A. (2013), Experimental investigation of the passive Earth pressure on retaining wall when the backfill is collapsible soil, doctoral dissertation, Concordia Univ., Montreal.
Puzrin, A. M., and A. Schmid (2007), TRIVEC measurements in the inverse analysis of the long-term stability of a constrained landslide, *Proceedings of the 7th International Symposium on Field Measurements in Geomechanics Boston, FMGM 07, Massachusetts, USA*, pp. 1–12, doi:10.1061/40940(307)97.
Schwarz, M., F. Preti, F. Giadrossich, P. Lehmann, and D. Or (2010a), Quantifying the role of vegetation in slope stability: A case study in Tuscany (Italy), *Ecol. Eng.*, *36*, 285–291, doi:10.1016/j.ecoleng.2009. 06.014.
Schwarz, M., P. Lehmann, and D. Or (2010b), Quantifying lateral root reinforcement in steep slopes: From a bundle of roots to tree stands, *Earth Surf. Processes Landforms*, *35*, 354–367.
Schwarz, M., D. Cohen, and D. Or (2011), Pullout tests of root analogs and natural root bundles in soil: Experiments and modeling, *J. Geophys. Res.*, *116*, F02007, doi:10.1029/2010JF001753.
Schwarz, M., J.-J. Thormann, K. Zürcher, and K. Feller (2012a), Quantifying root reinforcement in protection forests: Implications for slope stability and forest management, *Conference Proceedings, INTERPRAEVENT 2012*, Grenoble, France.
Schwarz, M., D. Cohen, and D. Or (2012b), Spatial characterization of root reinforcement at stand scale: Theory and case study, *Geomorphology*, *171*, 190–200.
Schwarz, M., F. Giadrossich, and D. Cohen (2013a), Modeling root reinforcement using a root-failure Weibull survival function, *Hydrol. Earth Syst. Sci.*, *17*, 4367–4377.
Schwarz, M., J.-J. Thormann, and K. Feller (2013b), Entwicklung und Validierung einer neuen Methode für die Beurteilung und Planung der minimalen Schutzwaldpflege auf rutschgefährdeten Hängen, final report for the Wald- und Holzforschungsfond, Swiss Federal Office for the Environment FOEN.
Shamsabadi, A., K. M. Rollins, and M. Kapuskar (2007), Nonlinear soil abutment bridge structure interaction for seismic performance-based design, *J. Geotech. Geoenviron.*, *133*, 707–720.
Shields, D. H., and A. Z. Tolunay (1973), Passive pressure coefficients by method of slices, *J. Soil Mech. Found. Div.*, *99*, 1043–1053.
Stokes, A., et al. (2014), Ecological mitigation of hillslope instability: Ten key issues facing researchers and practitioners, *Plant Soil*, *377*, 1–23.
Terwilliger, V. J., and L. J. Waldron (1991), Effects of root reinforcement on soil-slip patterns in the Transverse Ranges of Southern California, *Geol. Soc. Am. Bull.*, *103*, 775–785.
Timoshenko, S. P., and J. M. Gere (1961), *Theory of Elasticity Stability*, McGraw-Hill, New York.
Urciuoli, G., L. Picarelli, and S. Leroueil (2007), Local soil failure before general slope failure, *Geotech. Geol. Eng.*, *25*, 103–122.
Vergani, C., M. Schwarz, D. Cohen, J. J. Thormann, and G. B. Bischetti (2014), Effects of root tensile force and diameter distribution variability on root reinforcement in the Swiss and Italian Alps, *Can. J. For. Res.*, *44*, 1426–1440.
Waldron, L. J., and S. Dakessian (1981), Soil reinforcement by roots: Calculation of increased soil shear resistance from root properties, *Soil Sci.*, *132*, 427–435.
Wilson, P., and A. Elgamal (2010), Large-scale passive Earth pressure load-displacement tests and numerical simulation, *J. Geotech. Geoenviron.*, *136*, 1634–1643.
Wu, T. H., W. P. McKinnell III, and D. N. Swanston (1979), Strength of tree roots and landslides on Prince of Wales Island, Alaska, *Can. Geotech. J.*, *16*, 19–33.
Wu, T. H., R. M. McOmber, R. T. Erb, and P. E. Beal (1988), Study of soil-root interaction, *J. Geotech. Eng.*, *114*, 1351–1375.
Zeh, H. (2007), *Soil Bioengineering Construction Type Manual*, European Federation for Soil Bioengineering, Zürich.